Effect of annealing on the structural, optical and electrical properties of ITO films by RF sputtering under low vacuum level

T.S. Sathiaraj *

Physics Department, University of Botswana, P. Bag 0022, Gaborone, Botswana

ARTICLE INFO

Article history:
Received 7 March 2008
Accepted 14 June 2008
Available online 29 July 2008

PACS:
81.15.Cd
78.66.Li
73.61.Le
68.55.J

Keywords:
Indium tin oxide (ITO)
Sputtering
Optical properties
Electrical properties
X-ray diffraction
Annealing

ABSTRACT

Indium tin oxide (ITO) thin films were prepared by RF sputtering of ceramic ITO target in pure argon atmosphere at a high base pressure of 3×10^{-4} mbar without substrate heating and oxygen admittance. The use of pure argon during deposition resulted in films with high transparency (80–85%) in the visible and IR wavelength region. The films were subsequently annealed in air in the temperature range 100–400 °C. The annealed films show decreased transmittance in the IR region and decreased resistivity. The films were characterized by electron microscopy, spectrophotometry and XRD. The predominant orientation of the films is (2 2 2) instead of (4 0 0). The transmission and reflection spectra in the wavelength range 300–2500 nm are used to study the optical behaviour of the films. The optical transmittance and reflectance spectra of the films were simultaneously simulated with different dielectric function models. The best fit of the spectrophotometric data was obtained using the frequency-dependent damping constant in the Drude model coupled with the Bruggeman effective medium theory for the surface roughness. It has been found that the sputtering power and the chamber residual pressure play a key role in the resulting optical properties. This paper presents the refractive index profile, the structure determined from the XRD and the electrical properties of ITO films. It has been found from the electrical measurement that films sputtered at 200 W power and subsequently annealed at 400 °C have a sheet resistance of 80 Ω/□ and resistivity of 1.9×10^{-3} Ωcm.

© 2008 Elsevier Ltd. All rights reserved.

1. Introduction

Tin-doped indium oxide thin films have potential application as transparent conducting materials in flat panel displays [1] and in optoelectronic devices [2,3], because of their well-known physical properties such as low resistivity and high transmittance (T) in the visible wavelength region. Indium tin oxide (ITO) films have been prepared by different techniques such as spray pyrolysis, electron beam evaporation and sputtering to name a few. The sputtering technique is frequently used due to its good reproducibility, high deposition rate and good adhesion of the coatings to the substrate. Typically, magnetron sputtering processes are performed at a base pressure of $\approx 1.0 \times 10^{-5}$ mbar or high, high substrate temperature (>200 °C) with the introduction of O_2 into the gas mixture. The values of O_2 to Ar concentration are not univocally accepted with reports ranging from 0.1% to 10%. Zebaze Kana et al. [4] reported that the residual pressure in the chamber plays a key role in the resulting optical and electrical properties of the films. It has been found that the residual pressure is related to the water vapour out gassing from the vacuum system and its contribution to the chamber atmosphere can be equivalent to the intentional admittance of oxygen or water vapour into the system to have good-quality films. The literature is abundant with reports on the effect of sputtering conditions, oxygen partial pressure, target–substrate distance and post-deposition annealing on the optical, electrical and structural properties of ITO films. There is no detailed study done on the optical, electrical and structural properties of films deposited under high base pressure without substrate heating and intentional oxygen admittance. There is a clear correlation between the chamber residual pressure, substrate temperature, resistivity, transmittance and carrier mobility of sputtered ITO films [5]. For good reproducibility of the electrical and optical properties, it is important to understand the properties of ITO films prepared under high base pressure without oxygen admittance and substrate heating. In order to investigate the role of chamber residual pressure on ITO film properties, we prepared the samples at a high base pressure of 3×10^{-4} mbar, without oxygen admittance during sputtering. The value has been reached after studying different parameters during deposition.

Optical properties of thin films depend on process conditions. It is not sufficient to optically characterise thin films with either the Transmittance and Reflectance spectrum or one of them alone. Optical properties of ITO films can vary widely with deposition

* Tel.: +267 355 2461; fax: +267 318 5097.
E-mail address: sathiara@mopipi.ub.bw

conditions and post-deposition annealing. Since ITO films are found to have graded microstructure, proper study on the optical behaviour of the films involve the determination of optical constants namely the refractive index n and the extinction coefficient k over the spectral range of interest. The quantities n and k cannot be measured directly. Instead we measure properties such as reflectance and transmittance, or the ellipsometric parameters psi and delta. Then the desired quantities n and k can be extracted either by a theoretical model of the thin film or by techniques such as direct inversion of the experimental spectra, envelope method, etc. Conventional spectrophotometers can only make one measurement at a time and switching from one type of measurement to the other requires that the instrument be reconfigured. Usually, special accessories need to be purchased to adapt a transmittance spectrophotometer for reflectance measurements. With such a system, it is impossible to make both transmittance and reflectance measurements exactly at the same part of the sample. Therefore, conventionally only a single spectrum (either transmittance or reflection) is analysed. The envelope method is a preferred technique for analysing a single spectrum. It has the advantage that it is relatively stable and immune to imprecision in the measured data. However, this technique can only be applied to relatively thick non-absorbing materials, which has several peaks and valleys in the spectrum. Usually, the closeness of fit between the calculated and measured performance is taken as an indication of the reliability of the process. To have a reliable and accurate knowledge of the optical properties of ITO films it is important to use both the transmittance and reflectance spectrum over a wide spectral range for optical constants determination. Many works have been published on the use of spectroscopic ellipsometry for determining the optical constants n and k of the ITO films [6–8]. Relatively few reports have been published using spectrophotometric data to extract the optical constants [9,10]. In the present work, we present the results of modeling simultaneously the reflectance and transmittance spectra of ITO films deposited on glass substrates and subsequently annealed in air by using different dielectric models. The influence of sputtering power and annealing temperature on electrical and structural properties are also presented.

2. Experimental and computational methods

2.1. Sample preparation and characterisation

ITO films of various thicknesses are deposited on glass substrates by RF magnetron sputtering from an oxide ceramic target 90 wt% In_2O_3 and 10 wt% SnO_2(Kurt J. Lesker, USA) of 99.90% purity and 100 mm diameter. The depositing system (Edwards Auto 500) consists of a stainless steel chamber evacuated by an oil diffusion pump with liquid nitrogen trap. The chamber was evacuated to a base pressure of 3×10^{-4} mbar. The pressure during deposition was 1.2×10^{-2} mbar or less. Mass flow-controlled pure argon (99.99%) was delivered to the chamber at a flux of 16 sccm. The substrate to target distance was 13 cm. Two different sputtering powers 100 and 200 W were used. The thickness and surface roughness were measured by KLA Tencor P15 surface profiler. The transmittance (T) and specular reflectance (R) of the films were recorded with Cary500 UV–VIS–NIR spectrophotometer in the 300–2500 nm wavelength range. The SEM analysis was performed with Philips XL 30 ESEM attached with EDAX system. The structural properties were determined by X-ray diffraction (XRD) using a Philips PW3710 mpd-controlled XRD system with a PW1830 generator. The sheet resistance and the resistivity of the samples were calculated by the four-point probe method.

2.2. Optical modelling

The near normal reflectance and transmittance of the samples coated on micro glass slide, recorded from the spectrophotometer is used to extract the optical constants n and k of the coatings by spectra simulation. The fitting of model dielectric functions to the transmission and reflectance was performed by the commercially available software Scout2 [11].

2.3. Theoretical background

2.3.1. Dielectric modelling

In this dielectric modelling the optical properties of the ITO samples were represented by the following procedure. The dielectric function ε which relates the dielectric displacement D and the electric field vector can be written as [9]

$$D=\varepsilon_0\varepsilon E,$$

where $\varepsilon=1+\chi$ and χ is the susceptibility.

We can write the polarization of the medium as

$$P=\varepsilon_0\chi E$$

The complex dielectric function ε is given as $\varepsilon=\varepsilon_{re}+\varepsilon_{im}=1+\sum\chi_i$, where χ_i is the result of various mechanisms of polarization.

The complex refractive index is given as

$$N=n+ik=\sqrt{\varepsilon_{re}+\varepsilon_{im}}$$

where n is the refractive index and k is the extinction coefficient.

We can write the reflectance and transmittance of an absorbing film on a non-absorbing substrate in the form

$$R=r(n,k,n_0,n_s,d,\lambda)$$

$$T=t(n,k,n_0,n_s,d,\lambda)$$

where n and k are the refractive indices of the film, n_0 and n_s are those of the surrounding medium and substrate, d is the thickness and λ is the wavelength.

By knowing the refractive index n and the extinction coefficient k the reflectance and transmittance of the film can be calculated straightforward in the spectral region provided the thickness is known. But the inversion problem of finding the n and k from experimental R and T measurement involves several steps. A model dielectric function is constructed which consists of a constant dielectric background contributing to the real part of the dielectric function, and for the interband transition the OJL [12] model is employed where the expression for the joint density of states are given for the optical transition from the valence band to the conduction band. The imaginary part of χ thus calculated is used to obtain the real part by a Kramers–Kronig transformation. This also provides the consistency of the model with KK relation. A simple harmonic oscillator model was implemented for the interband transitions into the upper half of the conduction band. The classical Drude model was used for the susceptibility of the free electrons for the transitions into the conduction band.

The real and imaginary parts of the dielectric constant by the Drude model is

$$\varepsilon_{re}(\omega)=\varepsilon_\infty\left[1-\frac{\omega_p^2}{\omega^2+\Gamma^2}\right]$$

$$\varepsilon_{im}(\omega)=\varepsilon_\infty\frac{\Gamma}{\omega}\left[\frac{\omega_p^2}{\omega^2+\Gamma}\right]$$

where ω_p is the plasma frequency, ε_∞ the high-frequency dielectric constant, Γ is the damping constant. The dielectric background accounts for contributions to the dielectric function outside of the simulated wavelength range which is represented by ε_∞.

The following steps were followed in the simulation of the R and T spectra of the ITO films:

1. Formulation of the dielectric function as mentioned above.
2. The stack of layers is constructed either assuming a single layer or multilayer on a transparent (glass) substrate.
3. Initial values of the free parameters, substrate dielectric function and the estimated thickness from the surface profiler are entered.
4. T and R spectra are computed by assuming single or multilayer structure. The free parameters and thickness were varied to achieve the best fit by minimizing the deviation (mean squared difference) between simulated and measured spectra by the downhill simplex method.

The fit parameters in the above model are as follows. For the Drude model ω_p, ε_∞, Γ and for the OJl model the band gap energy, the tail state exponent and the strength of the transition.

2.3.2. Refined Drude model with frequency-dependent damping

In order to get better fit for the annealed samples whose free carriers damping exhibit dependence on the frequency, we used the extended Drude model where the damping factor is given as

$$\Gamma_{Dr}(\omega) = \Gamma_L - \left[\frac{\Gamma_L - \Gamma_H}{\pi}\right]\left(\arctan\left[\frac{\omega - \Omega_{\Gamma Dr}}{\Gamma_{\Gamma w}}\right] + \frac{\pi}{2}\right)$$

where Γ_L and Γ_H are the low and high-frequency damping constants, $\Gamma_{\Gamma w}$, $\Omega_{\Gamma Dr}$ are the width and the changeover frequency, respectively. The fit parameters are the ω_p, Γ_L, Γ_H, $\Gamma_{\Gamma w}$ and $\Omega_{\Gamma Dr}$. Once the plasma frequency is obtained from the fitting procedure the carrier density can be obtained via $n_e = (\omega_p^2 m * \varepsilon_0/e^2)$ where ε_0 is the permittivity of free space, e is the elementary charge and m^* is the effective mass and has been assumed a value of $m^* = 0.4m_0$, m_0 being the free electron mass.

2.3.3. Bruggemann model for the surface roughness

Since the growth process of ITO layers on glass substrates are not homogeneous especially on glass substrates [13], the experimental spectra were simulated with an additional surface roughness layer whose dielectric function is modelled with the effective medium approximation. The surface roughness layer is generally modelled with the Maxwell–Garnett [14] or Bruggeman [15] effective medium theories. This approach has been found to yield very accurate and reliable results in spectroscopic ellipsometry [6,7]. For the modelling, we constructed a two-layer structure on glass substrate with the top surface roughness layer. The surface layer was constructed as a composite of the ITO layer and voids (air). The effective dielectric function of the surface layer was computed using the dielectric function of the ITO layer and air by Bruggeman effective medium approximation. The volume fraction of the surface layer, thickness of the surface and ITO layer are used as fit parameters.

3. Results

3.1. Structural properties

Fig. 1 shows the XRD pattern of ITO thin films annealed at various temperatures sputter deposited at 100 W. The as-deposited films are polycrystalline with peaks corresponding to (2 2 2) and (4 4 0) orientations of In_2O_3. The predominant orientation is (2 2 2) in both cases of films deposited at 100 and 200 W discharge power indicating that the films have (1 1 1) preferential orientation. Though the crystallization temperature for ITO is reported to be 150 °C [16,17], the as-deposited films in this study show prominent (2 2 2) peaks. Sufficient thermal energy is necessary for crystallization during deposition and the substrate temperature during deposition which was monitored at the back of the substrate did not increase beyond 30 °C due to the long target–substrate distance (13 cm). In the absence of external heating the crystallization in the present study is due to the energy supply by the continuous energetic ion bombardment as reported by Park et al. [18]. They have observed that amorphous substrate might retard crystallization at the point adjacent to the substrate, but will allow crystallization at a place away from the substrate. So, crystallization will be more pronounced in thicker films deposited by continuous sputtering. In the present study, films were deposited on glass (amorphous) substrates. So, crystallization might be easier in thicker films. This was also verified by comparing films of higher thicknesses (deposited for longer time) under the same conditions. Fig. 2 is the XRD pattern of two films (210 and 600 nm thick) deposited at 100 W power and

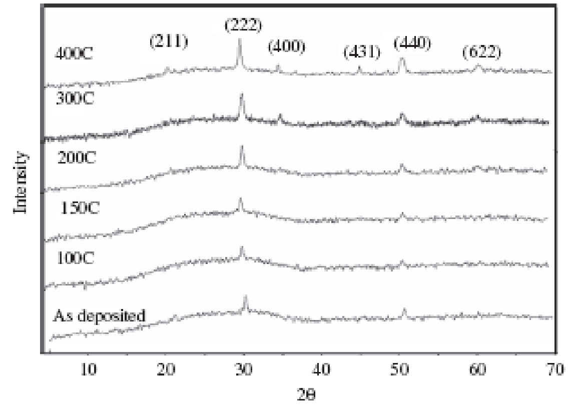

Fig. 1. XRD pattern of ITO films deposited at 100 W RF power on glass substrate at different annealing temperatures.

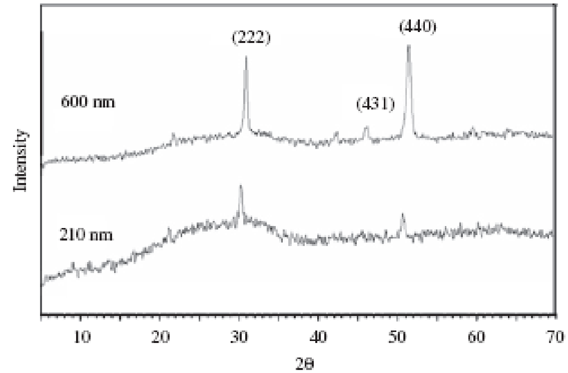

Fig. 2. XRD pattern of ITO films deposited at 100 W RF power on glass substrate at room temperature with different thicknesses.

can be seen that the thicker film deposited at room temperature has very intense peak at (2 2 2) than the thinner one. The kinetic energy from the sputtered particles enhances the surface migration which results in crystallization even at room-temperature sputtering conditions [19,20] and the crystallization is more pronounced in thicker films.

It is not observed in the present study any change in preferential orientation from the (2 2 2) to the (4 0 0) direction when the RF power (power density–deposition rate) is increased from 100 W (1.27 W/cm^2–35 Å/min) to 200 W (2.54 W/cm^2–81 Å/min), as reported by Thilakan et al. [21]. The as-deposited films at both power show the (2 2 2) and (4 4 0) peaks only. The (4 0 0) peaks appear in annealed films only above 200 °C and the intensity is very small compared to (2 2 2) peak. It has been reported that the presence of (4 0 0) orientation is related to the oxygen deficiency in the ITO films [22] and the preferential growth along the (2 2 2) direction is related to the stoichiometric ratio of In_2O_3, as observed by Terzini et al. [23] and the target–substrate distance [24]. In the present work, the films are deposited with high base pressure of 3×10^{-4} mbar, there is enough oxygen during deposition which resulted in films oriented along the (2 2 2) direction due to oxygen incorporation and since the target–substrate distance was large (13 cm); it has resulted in stoichiometric films. Our analysis with EDAX using the target as the standard shows that the as-deposited films are stoichiometric with 95 wt% In_2O_3 and 5 wt% SnO_2. As the films annealed above 200 °C show the crystallization along the (2 2 2) (4 0 0) (4 4 0) (4 3 1) (6 2 2) and (2 1 1) directions, it can be concluded that annealing above 200 °C results in oxygen deficiency, hence the appearance of the (4 0 0) peak.

The lattice constant a was calculated using the equation $1/d^2 = h^2{+}k^2{+}l^2/a^2$ and the grain size D by the Debye–Scherrer formula $D = (0.9\lambda/B\cos\theta)$, where d is the interplanar spacing, B is the measured broadening at half its maximum intensity (FWHM) at angle 2θ and X-ray wavelength $\lambda = 0.154$ nm.

The grain size and the lattice parameter calculated from the XRD peak (2 2 2) are plotted against the annealing temperature in Fig. 3. The grain size increases from 30 to 60 nm with the annealing temperature and matches with the reported values [25,26]. The increase in the degree of crystallinity is demonstrated by the increase in the grain size with annealing temperature.

The net lattice expansion can be defined as $\varepsilon_{net} = d{-}d_0/d_0$, where d is the interplanar spacing obtained from the XRD peak (2 2 2) position and d_0 is the interplanar spacing calculated from the lattice constant of 10.118 Å for the ideal lattice of In_2O_3 [27]. The resulting strain (net) with annealing temperature in this study is ranging from 0% to 1.5%, which is similar to the reported values for dc magnetron-sputtered films [28]. The strain is generally larger for the films deposited at 100 W power than those deposited at 200 W RF power. The values of the lattice constants are close to those reported [25,29], which was 10.102. The lattice constant decreases with annealing temperature T and equals that of the ideal value at 150 °C (100 W RF power) and 100 °C (200 W RF power) and the stress is also minimum after annealing at these temperatures which is similar to the observations made by Kerkache et al. [30] for RF-sputtered films.

3.2. *Optical properties*

Fig. 4a and b shows the transmittance and reflectance spectra of ITO films deposited at sputtering power 100 and 200 W and heated at various temperatures in air. It can be seen from the above figures that the use of pure Ar during sputtering result in the deposition of highly transparent films due to the high base pressure [4], in our case 3×10^{-4} mbar. As can be seen from the figure, just after deposition, the film with a high transparency in all intervals of wavelengths (300–2500 nm) is obtained for both sputtering powers. Further annealing in air does not result in the essential change of film transparency in the visible region. In the near IR region annealing in air above 150 °C (power 100 W) and above 200 °C (power 200 W) resulted in the decrease of transparency with the wavelength. The shifts in the transmittance and reflectance fringes of the annealed samples suggest that annealing results in a small change in the thickness or in the refractive index of the films.

There is a minimal change in transparency in the visible region after annealing at various temperatures following the first annealing stage and no noticeable change thereafter. This change is a shift of the transmittance and reflectance curve to the left of the X-axis, i.e. towards shorter wavelength/higher energy. The transmittance above 2000 nm decreases after annealing at 200 °C and increases after annealing at 300 and 400 °C. Other investigators have reported conflicting effects of heating on the transmittance of ITO: while Haines et al. [31] and Neubert et al. [32] report a decrease in transmission due to heating, Higuchi et al. [33],

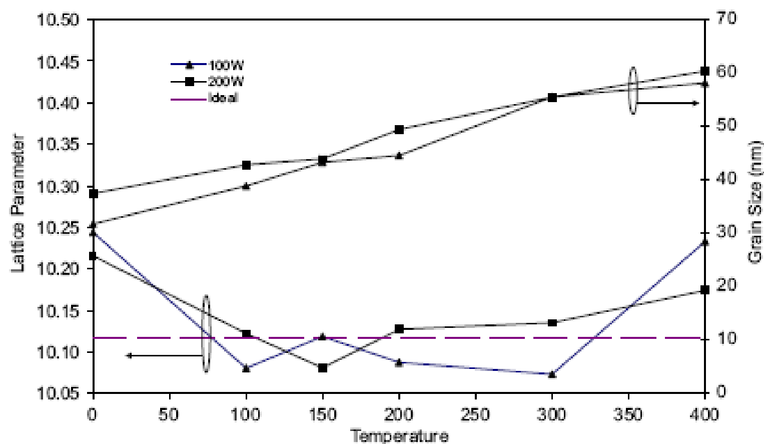

Fig. 3. Variations of lattice parameter and grain size of ITO films with different annealing temperatures.

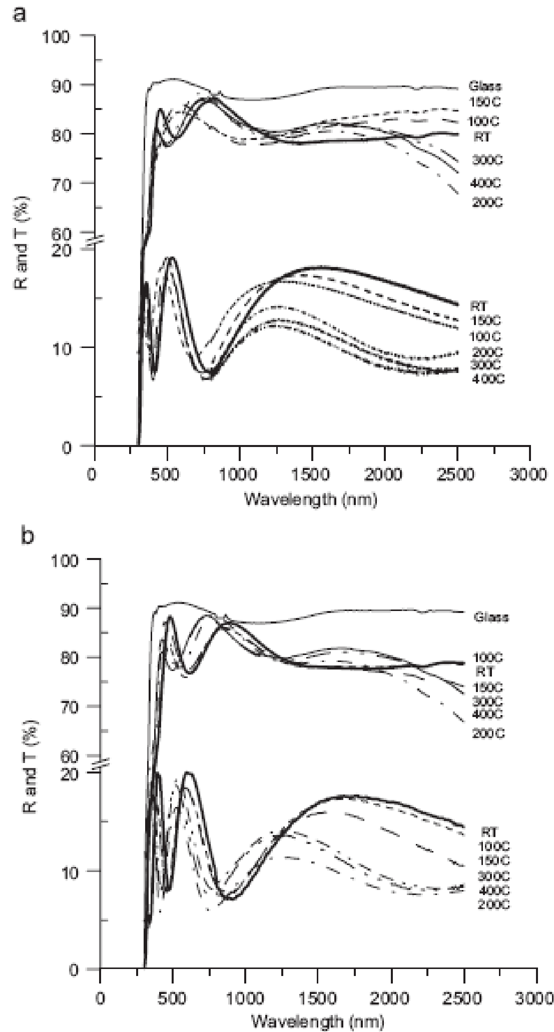

Fig. 4. . (a) Transmission (T) and reflection (R) spectra of ITO films on glass substrate deposited at 100 W RF power and (b) transmission (T) and reflection (R) spectra of ITO films on glass substrate deposited at 200 W RF power.

Sreenivas et al. [34], Ali et al. [35] and Hu et al. [36] observe an increase after annealing. These conflicts are most likely due to their differing methods of ITO growth and post-deposition treatments. The factors that affect the optical behaviour during post-deposition annealing of ITO films are the base pressure before sputtering, oxygen partial pressure during sputtering and the substrate heating. Since the oxygen content in ITO films is a critical control parameter [37] of the resistivity and transparency of the film, a small quantity of oxygen (usually a fraction of a percent) is usually added to the gas mixture in the sputtering of ITO from an ITO source. Conduction is partially a result of unfilled oxygen vacancies, so a high incorporation of oxygen into the film will result in few vacancies and a highly resistive film. In the present work, due to the base pressure being high, it resulted in a high level of oxygen incorporation and the subsequent high transparent and high resistive films.

The present experimental transmittance curves are very similar to the reported annealed ITO films prepared by dc reactive sputtering at room temperature with high oxygen partial pressure 11.7×10^{-4} mbar by Meng et al. [38]. The XRD of the reported ITO films by Meng et al. also show preferential orientation along the (2 2 2) direction and there is no (4 0 0) peak observed even after annealing at 400 °C.

Experimental transmittance and reflectance spectra in the spectral range 300–2500 nm have been fitted with the theoretical ones based on dielectric modeling. Optical, electrical and physical parameters, such as, the band gap, the electron concentration, mobility and the film thickness were obtained from the fitting.

Fig. 5 shows the typical fit obtained for an ITO sample deposited at 200 W RF power and subsequently annealed at 200 °C by Drude and the extended Drude model with frequency-dependent damping. It was arrived by assuming two layers on a glass substrate. The dielectric function of the glass substrate (micro slide) which was determined in the wavelength of interest from its near normal reflectance and transmittance is used in the layer model. We assumed incoherent interference and negligible absorption for the thick glass substrate. The dielectric function of the layer in first approximation, modelled with the standard Drude formula as discussed before. When the same double layer model on glass substrate with Drude theory was used for films annealed at 200 °C and above, the average experimental spectrum is well reproduced as we see from Fig. 5. The position of interference maxima and minima matches the model, but the fit between experimental and simulated ones at longer wavelengths are not matched in amplitude. Better fit could be achieved only by incorporating the frequency-dependent damping constant in the Drude model. The experimental and model spectra by the classical Drude model and the refined (extended) Drude model are shown in the figure for a 250-nm-thick film deposited at 200 W. As we see from the figure, the agreement between the simulated and the experimental spectrum has considerably improved. This trend was observed on all samples annealed above 200 °C temperature. It is clearly seen that the introduction of a frequency dependence damping constant in the Drude model, significantly improves the fit in the full range of wavelength studied. In this present study, all

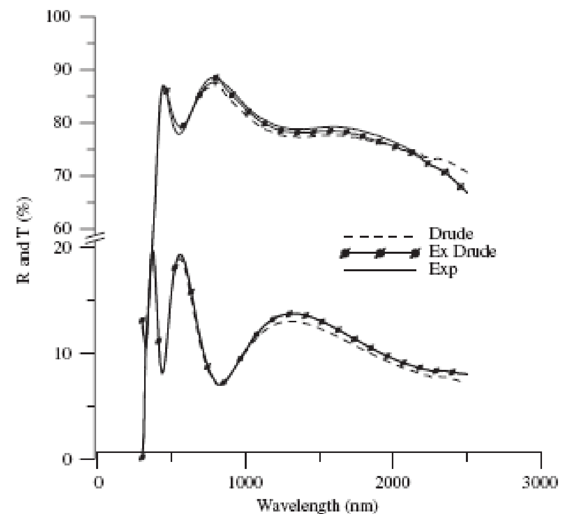

Fig. 5. Measured and calculated R and T spectra of ITO film deposited at 200 W RF power and annealed at 200 C with Drude and extended Drude model.

the experimental reflectance and transmittance spectra were fitted with the extended Drude model only.

In Figs. 6 and 7, we present the variation in optical constants of the ITO films annealed at different temperatures obtained by the dielectric modelling. Higher annealing temperatures resulted in lower refractive indices. Crystallographic orientation of the ITO films shows a clear relationship with refractive indices. As the films were annealed they become denser (larger grain size) and have lower refractive indices.

The changes in extinction coefficients are quite different between the visible range (about 400–700 nm) and the near infrared region (above 700 nm). In the visible range, the extinction coefficients were lower for higher annealing temperature conditions and in the longer wavelength region, higher annealing temperature led to larger extinction coefficients.

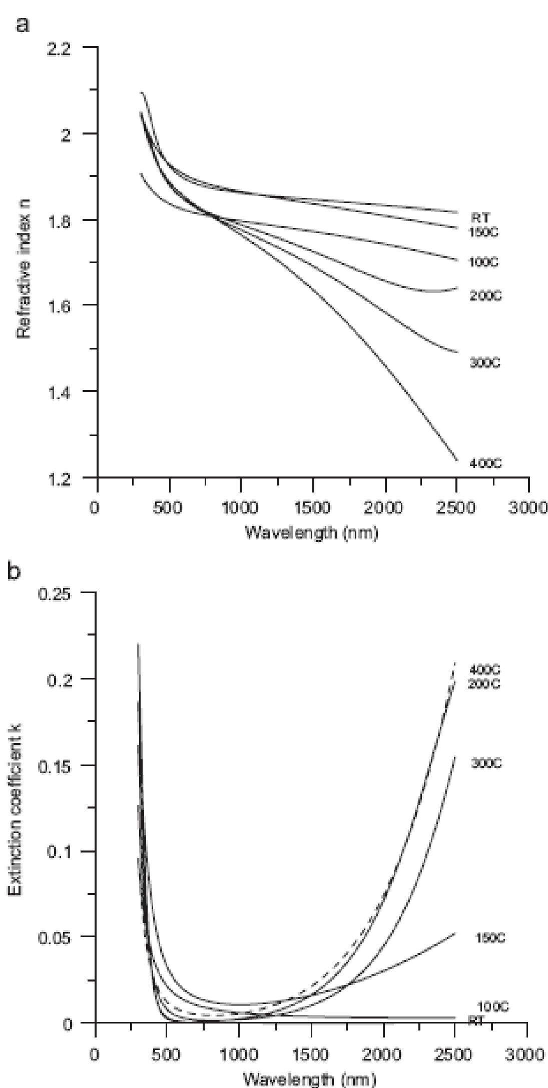

Fig. 6. Variation of (a) refractive index and (b) extinction coefficient of ITO films deposited at 100 W RF power with different annealing temperatures.

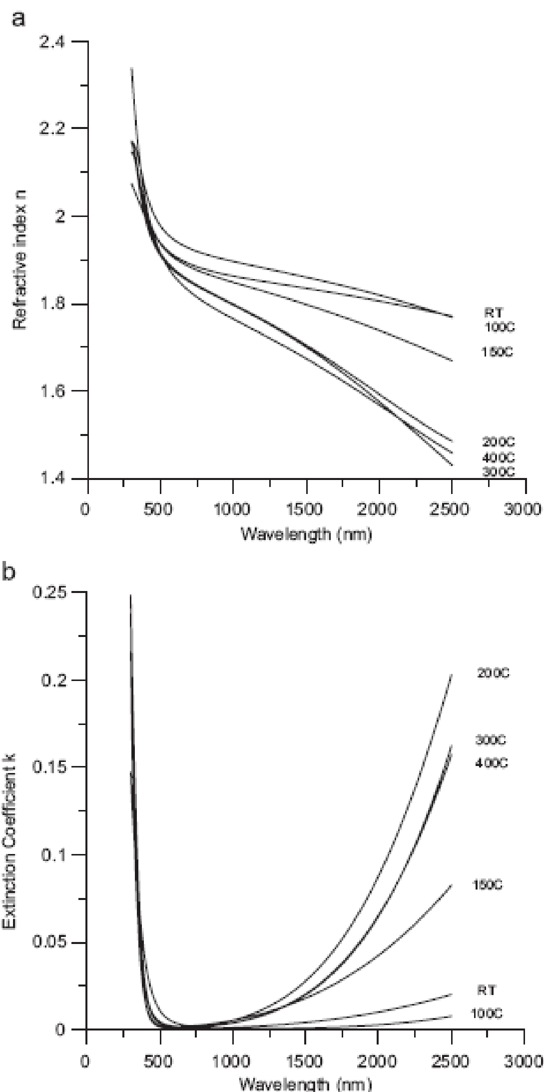

Fig. 7. Variation of (a) refractive index and (b) extinction coefficient of ITO films deposited at 200 W RF power with different annealing temperatures.

The extinction coefficient in this region exhibit a sharp increase with wavelength and temperature and can be observed that the increase is maximum for samples annealed at 200 °C. Since the extinction coefficient account for the absorption in the longer wavelengths, the higher the extinction coefficient, lower the transmittance, larger the absorption and high electron concentration [39].

With the dielectric modelling, information regarding the band gap, thickness, carrier concentration and void distribution in the surface layer was also obtained. Fig. 8a and b shows the variation of carrier density and band gap with the annealing temperature. The carrier concentration is higher for films deposited at 200 W RF power, which is consistent with the reported results [24]. The

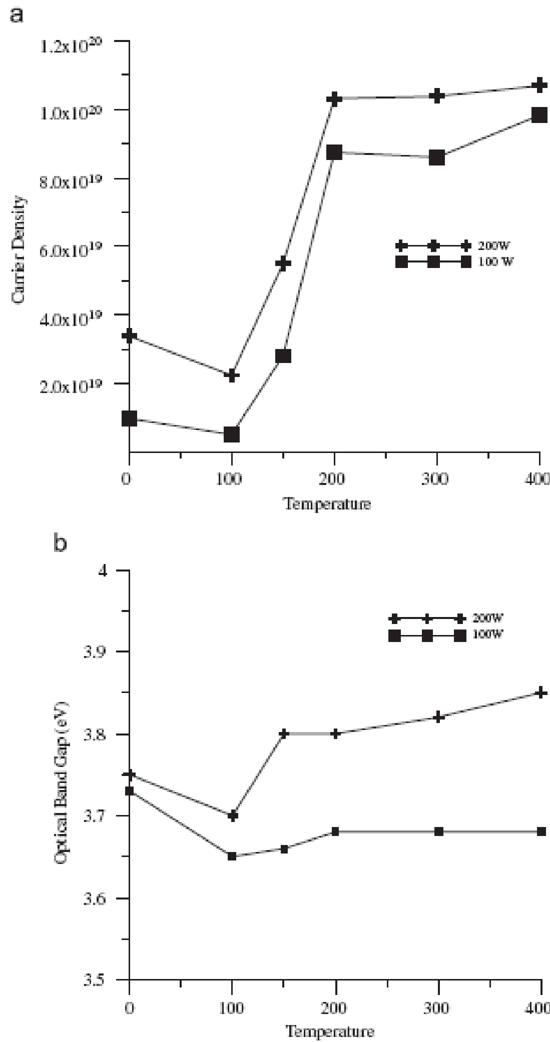

Fig. 8. Variations of (a) carrier density and (b) the optical band gap of ITO films with the annealing temperatures.

optical band gap of the films was calculated from the absorption spectra obtained from the extinction coefficient. It is assumed that the material has parabolic band structure and the direct optical band gap was determined from the plot of $(\alpha h\upsilon)^2$ vs. $h\upsilon$ extrapolated the linear portion of the curve to $\alpha h\upsilon$ equal to zero. Films deposited at 200W RF power have higher optical band gap than with those deposited at 100 W RF power. The band gap of the films lies between 3.6 and 3.9 eV. Vasant kumar et al. [24] have obtained a direct optical band gap of 3.7 eV for RF-sputtered ITO films with (2 2 2) preferential orientation and 3.5 eV for films with (4 4 0) preferential orientation. The films in this present study have been found to have (2 2 2) preferential orientation, and the range of band gap obtained matches with their report. The band gap decrease after annealing at 100 °C and then increased with the increase of annealing temperature. The band gap broadening can be attributed to the Burstein–Moss shift [40] as the result of high concentration of free electrons, as shown in Fig. 8a.

3.3. Electrical properties

Fig. 9a and b shows the sheet resistance and the resistivity of the films deposited at 100 and 200W RF power. The resistivity decreases as the annealing temperature increases. The electrical property of the films was found to be related to the microstructure and crystallinity of the films, which in turn strongly depend on the annealing temperature. Higuchi et al. [5] report that the low resistivity of ITO films is related to a big grain size. In this present study, annealing resulted in larger grain as shown in Fig. 3, which leads to less scattering at grain boundaries, hence lowered resistivity. Annealing above 100 °C led to a sharp increase in carrier concentration, which caused the subsequent decrease in sheet resistance and resistivity. The fall of resistivity may also be associated with the better crystallisation as seen from the increase in peak intensities with the annealing temperatures in the XRD, as shown in Fig. 1. Annealing above temperatures 400 °C show no

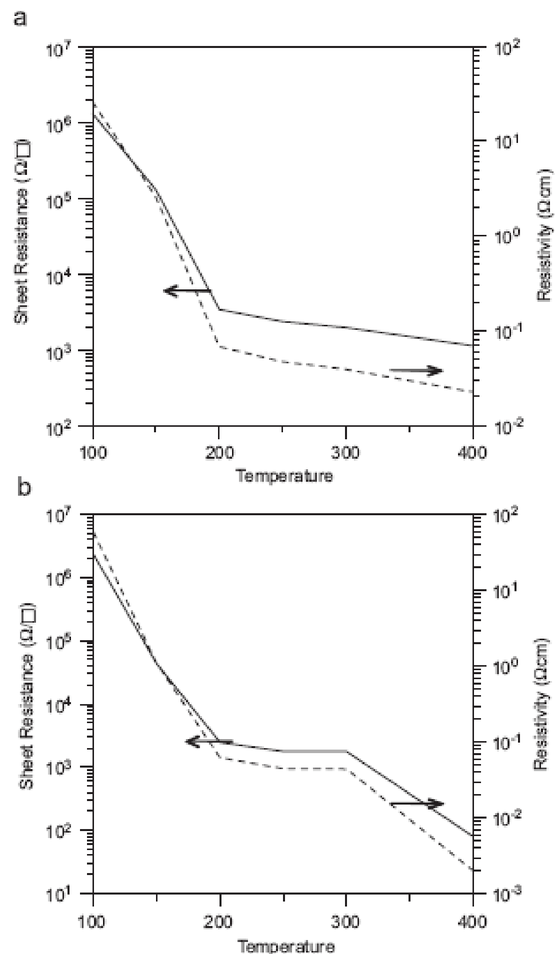

Fig. 9. Variations of sheet resistance and resistivity of ITO films deposited at (a) 100 W and (b) 200 W RF power with the annealing temperatures.

further effect on resistivity. As seen from the XRD, the (4 0 0) peaks appear only after annealing at 200 °C which is related to the oxygen deficiency and decrease in resistivity.

5. Conclusions

ITO films, grown on glass substrates by RF magnetron sputtering at a high chamber base pressure without substrate heating show high transparency in the 300–2500 nm wavelength region and are highly resistive. This is due to the high base pressure which plays the same role of the intentional oxygen admittance during sputtering. The as-deposited films were polycrystalline with preferential orientation along the (2 2 2) direction which also confirms that the films are stoichiometric. The subsequent annealing in air improves the crystallinity of the films which result in the growth of grain size. The resulting increase in carrier concentration decreases the resistivity of the films due to annealing. Higher grain size decreases the density which subsequently lowers the refractive index. The experimental transmittance and reflectance spectra in the wavelength interval 300–2500 nm is satisfactorily fitted by employing a theoretical model based on the frequency-dependent damping constant in the Drude model coupled with the Bruggeman effective medium theory for the surface roughness. The extracted optical constants have direct relation to the structural properties. The increase in carrier concentration with annealing temperature suggests that the films were becoming more metallic as evident from the increase in the extinction coefficient in the long wavelength region. No preferential orientation from the (2 2 2) to the (4 0 0) direction is observed in the present study when the RF power (deposition rate) is increased from 100 W (1.27 W/cm^2–35 Å/min) to 200 W (2.54 W/cm^2–81 Å/min), as reported in the literature. It has been found from the electrical measurement that films sputtered at 200 W power under the conditions detailed in the experimental setup and subsequently annealed at 400 °C have a sheet resistance of 80 Ω/□ and resistivity 1.9×10^{-3} Ωcm.

Acknowledgment

This work has been fully funded by the University of Botswana research grant R200.

References

[1] B.H. Lee, I.G. Kim, S.W. Cho, S.H. Lee, Thin Solid films 302 (1997) 25.
[2] G. Haacke, Annu. Rev. Mater. Sci. 7 (1977) 73.
[3] C.G. Granqvist, Appl. Phys. A. Mater. Sci. Process. 52 (1991) 83.
[4] M.G. Zebaze Kana, E. Centurioni, D. Iencinella, C. Summonte, Thin Solid Films 500 (2006) 203.
[5] M. Higuchi, S. Uekusa, R. Nakano, K. Yokogawa, Jpn. J. Appl. Phys. 74 (11) (1993) 6710.
[6] Yeon Sik Jung, Thin Solid Films 467 (2004) 36.
[7] R.A. Synowicki, Thin Solid films 313–314 (1998) 394.
[8] Y. Yang, X.W. Sun, B.J. Chen, C.X. Xu, T.P. Chen, C.Q. Sun, B.K. Tay, Z. Sun, Thin Solid films 510 (2006) 95.
[9] D. Mergel, Z. Qiao, J. Phys. D. Appl. Phys. 35 (2002) 794.
[10] A. Soleiman, M.A. Aegerter, Thin Solid Films 502 (2006) 205.
[11] M. Theiss, Hard- and Software for Optical Spectroscopy, Dr.-Bernhard-Klein-Str. 110, D-52078 Aachen, Germany
[12] S.K. O'Leary, S.R. Johnson, P.K. Lim, J. Appl. Phys. 82 (1997) 3334.
[13] A.V. Mudryi, A.V. Ivaniukovich, A.G. Ulyashin, Thin Solid Films 515 (2007) 6489.
[14] J.C. Maxwell-Garnett, Philos. Trans. R. Soc. A 205 (1906) 237.
[15] D.A.G. Bruggeman, Ann. Phys. Lpz. 24 (1935) 636.
[16] P.K. Song, Y. Shigesato, I. Yasui, C.W. Ow-Yang, D.C. Paine, Jpn. J. Appl. Phys. 37 (1998) 1870.
[17] T. Minami, H. Sonohara, T. Kakumu, S. Takata, Thin Solid Films 270 (1995) 37.
[18] Ju-O Park, Joon-Hyung Lee, Jeong-Joo Kim, Sang-Hee Cho, Young Ki Cho, Thin Solid Films 474 (2005) 127.
[19] Aldrin Antony, M. Nisha, R. Manoj, M.K. Jayaraj, Appl. Surf. Sci. 225 (2004) 294.
[20] P.K. Song, Y. Shiigesato, M. Kamei, I. Yasui, Jpn. J. Appl. Phys 38 (1999) 2921.
[21] P. Thilakan, C. Minarini, S. Ioreti, E. Terzini, Thin Solid Films 388 (2001) 34.
[22] D. Kim, Y. Han, J.S. Cho, S.K. Koh, Thin Solid Films 377–378 (2000) 81.
[23] E. Terzini, P. Thilakan, C. Minarini, Mater. Sci. Eng.—B 77 (2000) 110.
[24] C.V.R. Vasnt Kumar, A. Mansingh, J. Appl. Phys. 65 (1989) 1270.
[25] Hamid Reza Fallah, Mohsen Ghasemi, Ali Hassanzadeh, Hadi Steki, Physica B 373 (2006) 274.
[26] X.W. Sun, L.D. Wang, H.S. Kwok, Thin Solid Films 360 (2000) 75.
[27] R.N. Joshi, V.P. Singh, J.C. McClure, Thin Solid Films 257 (1995) 32.
[28] D. Mergel, Z. Qiao, J. Appl. Phys. 95 (2004) 5608.
[29] S. Naseem, I.A. Rauf, K. Hussain, N.A. Malik, Thin Solid Films 156 (1988) 161.
[30] L. Kerkache, A. Layadi, E. Dogheche, D. Remiens, J. Phys. D. Appl. Phys. 39 (2006) 184.
[31] W.G. Haines, R.H. Bube, J. Appl. Phys. 49 (1978) 304.
[32] T. Neubert, F. Neumann, K.P. Schiffmann, A. Willich, A. Hangleiter, Thin Solid Films 513 (2006) 319.
[33] M. Higuchi, S. Uekusa, R. Nakano, K. Yokogawa, Jpn. J. Appl. Phys. 33 (1994) 302.
[34] K. Sreenivas, T. Sundarsena Rao, A. Mansingh, S. Chandra, J. Appl. Phys. 57 (1985) 384.
[35] H.M. Ali, H.A. Mohamed, S.H. Mohamed, Eur. Phys. J. Appl. Phys. 31 (2005) 87.
[36] Yalan Hu, Xungang Diao, Cong Wang, Weichang Hao, Tianmin Wang, Vacuum 75 (2004) 183.
[37] J. Szczyrbowski, A. Dietrich, H. Hoffmann, Phys. Stat. Sol. A 78 (1983) 243.
[38] Li-Jian Meng, Frank Placido, Surf. Coat. Technol. 166 (2003) 44.
[39] C.G. Granqvist, A. Hultaker, Thin Solid Films 411 (2002) 1.
[40] E. Burstein, Phys. Rev. 93 (1954) 632.